JOURNAL OF AIRCRAFT
Vol. 34, No. 6, November–December 1997

Different Wings Flowfields Interaction on the Wing–Propeller Coupling

Rosario M. Ardito Marretta*
University of Palermo, Palermo 90128, Italy

A high-portability numerical technique based on the method of free wake analysis (FWA) is described that analyzes the interference between an aircraft propeller and a wing having different planforms and computes the influence of the wing aerodynamic field on the propeller performance. For an isolated propeller and wing, the models employed are based on the FWA and Prandtl theory, respectively. The performance of the propeller in the presence of the wing is related to the wing angle of attack and to the variation of wing circulation and the corresponding induced velocity at the propeller disk. A numerical model, previously and successfully used, was implemented to account for the effects of a wing on the wing–propeller coupling. To test the robustness of the method, the available experimental data obtained on a scale model of an isolated propeller are used. In a correlation study, the results, when wing and propeller are coupled, show the sensitivity of thrust, power, and efficiency to inflow conditions and blade pitch, as well as to the wing planform.

Nomenclature

A = tip vortex contraction coefficient, Eq. (2)
a = experimentally determined constant, Eq. (2)
B = number of blades
b = semispan, m
C_L = wing lift coefficient
C_P = power coefficient, $P/\rho n^3 D^5$
C_T = thrust coefficient, $T/\rho n^2 D^4$
c = wing chord, m
D = propeller diameter, m
H = induced velocity parameter, Eq. (8)
J = propeller advance ratio, U_∞/nD
K_1, K_2 = tip vortex translation coefficients, Eqs. (3) and (4)
n = blade rotational frequency, rps
$OXYZ$ = fixed coordinate system, Fig. 1
P = power of the propeller, $2\pi nQ$, W
Q = propeller torque, N m
q = velocity induced by the wing, m/s
R = radius of propeller, m
R_0 = radius of propeller hub, m
r_t = radial contraction of the tip vortex in the propeller wake, m
r_v = radial contraction of a vortex from point ξ on the blade, m
s = nondimensional wing span
T = thrust of the propeller, N
U_∞ = freestream velocity, m/s
u, v, w = velocity components, m/s
V_{ia} = velocity induced by sheet vortices, m/s
V_{il} = velocity induced by free vortices, m/s
x_t = axial convection of propeller tip vortex, m
x_v = axial convection of any vortex of the propeller wake, m
α = angle of attack, deg
β = propeller blade angle at 0.7, deg
Γ = circulation, m^2/s
ΔC_P = change in power coefficient
ΔC_T = change in thrust coefficient
$\Delta C_{\bar{T}}$ = source of vibration on the aircraft
η = efficiency of the propeller
θ = angular increment of blade rotation, deg
ξ = fraction of blade radius, r/R
ψ = azimuth coordinate in the propeller wake, deg
Ω = rotational speed, rad/s

Received Dec. 7, 1996; revision received June 18, 1997; accepted for publication June 23, 1997.

*Research Engineer, Department of Mechanics and Aeronautics; currently at University of Pisa, Department of Aerospace Engineering, Via Diotisalvi 2, Pisa 56126, Italy. Member AIAA.

Introduction

PREVIOUS studies of the coupling of a wing and propeller have focused on the complex local flows arising from the aerodynamic interaction between a tractor propeller and the wing on which it is mounted. In the present study, the aerodynamic field in the wake of the propeller has been analyzed. The free wake analysis (FWA) method, as will be demonstrated by comparison with new experimental results, has been successful in numerically predicting the wing–propeller interference.

The behavior and the mechanism of the interaction between the wing and propeller has been described by Witkowski et al.[1] by assuming that the flowfield is inviscid and quasisteady behind the propeller; Cho and Williams[2] and Rottgermann and Wagner[3] focused the problem on frequencies dominant in unsteady flows. Results presented by Catalano,[4] who made use of Konig's theory for a two-dimensional smooth wing and a pusher propeller, show the behavior of a propeller in this type of coupling. The isolated propeller was analyzed by Kinnas and Hsin[5] using the boundary element method (BEM). More recently, Yamaguchi and Bose[6] and Bose,[7] dealing with a two-dimensional time-domain constant potential panel method, highlighted the behavior of a propeller in oscillatory motions as well as in response to chordwise deflections of large amplitude. When the blade tip speed is low enough to not encounter compressible flow, the comparison with many of their results shows that the conclusions obtained by using the quasisteady model are similar to those of the more complex unsteady one.

Following Favier et al.,[8–10] Marretta,[11] and more recently, Chiaramonte et al.,[12] the isolated propeller and wing in a freestream are considered first, and the FWA method is then used to find the numerical results that form the basis for achieving a highly flexible numerical simulation of the mutual influence of the wing–propeller on the performance of the aircraft. By representing the wake and propeller blades by lifting lines,

more detailed results become available for the flow past the propeller. Moreover, to improve accuracy, instead of the classical Prandtl scheme, the theory from Pistolesi–Weissinger[13] is used, in which the bound vortex is placed at the wing quarter-chord line and the velocity tangency condition to the surface is imposed at the three-quarter-chord line. The approach is described in Refs. 14–16 and can be applied for a rectangular, trapezoidal, and swept-back wing, as well as for an elliptical one. By developing a complete numerical procedure, this may be applied successively to both the wing and propeller.[1,2,15] The variations of the performance characteristics of the tractor propeller are then developed in terms of the wing angle of attack, the variation of circulation, and the induced downwash near the propeller disk area for these different wing geometries. In that region, the inflow conditions at the propeller are altered by the wing, i.e., the propeller operating condition is changed. The results demonstrate that when compared to an isolated propeller, changes in thrust, torque or power, and efficiency become larger as α and β increase. The results also show the effects of the different inductions on the amplitude response of the previously mentioned parameters.

Propeller Wake Model

To find the solution to this aerodynamic problem, it is necessary to analyze and model the wake of the propeller blades. In this paper, the FWA approach is first applied to an isolated propeller. This iterative method is based on a convergence criterion imposed on the sheet of vortices leaving each blade to form the propeller wake. The wake sheet is modeled using the vortex lines starting from the points on the blade.[8–10] Following Favier et al.,[8] r_t and x_t are related to ψ and are valid in the region near the propeller disk, the so-called near wake; outside a value ψ_s (far wake), the region of flow becomes unstable (Fig. 1). The convection dominance of propeller flows like those of interest here makes this essentially irrelevant. The following equation relates the value of ψ_s to J, β, and B:

$$(\psi_s - \psi_B)/B \cdot \psi_B = 0.25[8.5 - \beta/10 - J \cdot (J + 2)] \quad (1)$$

where ψ_B is the angle between each blade, $=360/B$, J is the advance ratio, and β is the blade angle at $0.7R$. For the tip vortex paths, one obtains

$$r_t/R = A + (1 - a) \cdot e^{-\psi/B} \quad \text{for} \quad 0 \le \psi \le \psi_s \quad (2)$$

$$x_t/R = K_1 \cdot (\psi/\psi_B) \quad \text{for} \quad 0 \le \psi \le \psi_B \quad (3)$$

$$x_t/R = K_1 + K_2 \cdot (\psi/\psi_B - 1) \quad \text{for} \quad \psi_B \le \psi \le \psi_s \quad (4)$$

where A, K_1, and K_2 are related to β and J. By similarity, the relationship between r_v and r_t is

$$r_v/R = \xi \cdot r_t(\psi) \quad \text{for} \quad 0 \le \psi \le \psi_s \quad (5)$$

and for x_v, one obtains

$$x_v/R = H(r, 0) \cdot \psi \quad \text{for} \quad 0 \le \psi \le \psi_B \quad (6)$$

$$x_v/R = H(r, 0) \cdot \psi_B + H(r, \psi_B) \cdot (\psi - \psi_B) \quad \text{for} \quad \psi_B \le \psi \le \psi_s \quad (7)$$

where the functions $H(r, 0)$ and $H(r, \psi)$ depend on the coordinates of the vortex filament (ψ, ψ_B).

The velocities u, v, and w induced by the wing and its wake at any point on the blade P may be obtained by relating C_L to the wing and wake vortex strengths and by using the Kutta–Joukowski theorem. H may then be found as a function of the induced velocity components u, v, w, and ψ:

$$H(u, v, w, \psi, r) = (\pi/180) \cdot (U_\infty + u) \cdot \xi / (\Omega \cdot r + v \cdot \cos\psi - w \cdot \sin\psi) \quad (8)$$

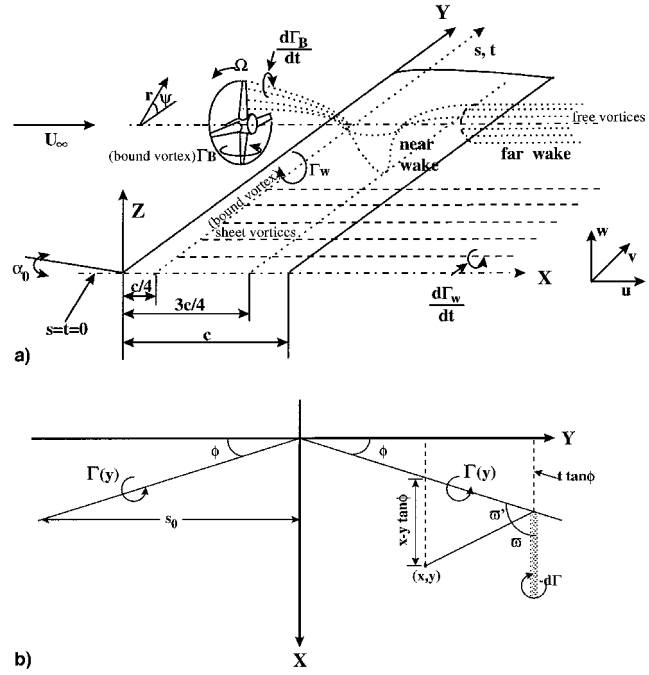

Fig. 1 a) Configuration of the wing-propeller geometry and wake (rectangular wing) and b) geometry and wake (swept-back wing).

Note that the induced velocity w will be given by Eq. (15). Through Biot–Savart's law, applied to the blade circulation $\Gamma(\xi)$, and the trailing wake vortices, one obtains the induced velocity at any point in the wake, as follows:

$$\boldsymbol{V}_P = \frac{1}{4\pi} \cdot \int_{R_0}^{R} \Gamma(\xi) \cdot \frac{\mathrm{d}\boldsymbol{l} \times \boldsymbol{r}}{|\boldsymbol{r}|^3} + \frac{1}{4\pi} \cdot \int_{\xi_0}^{1} \left[\frac{-\mathrm{d}\Gamma(\xi)}{\mathrm{d}\xi} \cdot \int_{L(\xi)} \frac{\mathrm{d}\boldsymbol{l} \times \boldsymbol{r}}{|\boldsymbol{r}|^3} \right] \cdot \mathrm{d}\xi \quad (9)$$

In Eq. (9), $\boldsymbol{r}$ represents the position vector of a space point P with respect to the vortex coordinate system, $L(\xi)$ is the vortex filament leaving the point ξ of the blade, and $\mathrm{d}\boldsymbol{l}$ is the vector parallel to the direction of the bound vortex in the first integral and to the trailing vortex filaments in the second one. By noting that the bound vortices ever influence the near-wake region, we suppose this influence may well not be large and $\mathrm{d}\boldsymbol{l} \times \boldsymbol{r}$ vanishes. Having determined Γ from Eq. (9), the velocity induced at the point P by the sheet vortices may be written as a superposition, on each blade, of each integral:

$$\boldsymbol{V}_{id}(P) = \frac{1}{4\pi} \cdot \sum_{p=1}^{B} \int_{\xi_0}^{1} \Gamma(\xi) \cdot \frac{\boldsymbol{\tau}_p \times \boldsymbol{r}_p}{|\boldsymbol{r}_p|^3} \cdot \mathrm{d}\xi \quad (10)$$

Where $\boldsymbol{\tau}_p$ is the vector parallel to the direction of the sheet vortex filament. Therefore, the velocity V_{il} induced by the free vortices at point P may be written as

$$\boldsymbol{V}_{il}(P) = \frac{1}{4\pi} \cdot \int_{R_0}^{R} \frac{\mathrm{d}\Gamma(\xi)}{\mathrm{d}\xi} \cdot \boldsymbol{G}(P, \xi) \cdot \mathrm{d}\xi \quad (11)$$

where the influence coefficients $\boldsymbol{G}(P, \xi)$ are expressed as

$$\boldsymbol{G}(P, \xi) = -\int_{Lp(\xi)} \sum_{p=1}^{B} \frac{\boldsymbol{\tau}_p \times \boldsymbol{r}_p}{|\boldsymbol{r}_p|^3} \cdot \mathrm{d}l \quad (12)$$

regarding the model development of the far-wake regions.[16] The strength assigned to the vortices of the far-wake region is that of the last vortices of the near-wake region.

Numerical Simulation

As previously done,[16] the propeller performance is calculated for a propeller with a given number of blades with specified dimensional and design characteristics β, the geometric twist, the diameters R and R_o, the freestream velocity, and Ω. The present work will take into account the strength of the different downwashes induced by three different wings and their interaction with the propeller performance in terms of amplitudes of the oscillations of thrust, torque, and efficiency. Based on previous literature concerning numerical results and experimental data,[8–11] the aerodynamic characteristics of the blade airfoil sections can be introduced. Specifically, a four-bladed propeller having hub and overall diameters of 0.4 m (1.31 ft) and 2.0 m (6.56 ft), respectively, is considered. The range of values of J is 0.2–0.8, and the mean blade pitch setting varies from 23 to 32.5 deg. For the rectangular wing it has been assumed that the distance between the propeller axis and wing midspan and the distance between the propeller disk and the wing leading edge were 2 m (6.56 ft) and 0.2 m (0.655 ft), respectively. In this paper, the blades have constant NACA 64A408 airfoil sections.

Through the iterative Newton–Raphson scheme, the previous nonlinear system, identified by Eqs. (2–4), is solved; the helix pitch vortex filaments or the axial spacing of the turns of helical wake is equal to the translation of the propeller per revolution, and the calculated velocity field becomes tangent at the points of each vortex line. The output of the model gives the velocity field, circulation distribution, wake geometry, and the performance characteristics of the propeller, namely C_T, C_P, and η (Figs. 2a–2c, 3a–3c, and 4). The purpose of the present investigation is to implement the behavior and mechanism of the interaction wing–propeller,[11,14–16] showing the effects of the presence of different wing geometries behind the propeller on the coefficients C_T, C_P, and η. The circulation related to the geometry of the wing also induces a velocity field on the wake of the propeller giving, in effect, a change in the direction of the wake and the advance ratio J. Because the wing circulation and induced velocities are related to the wing angle of attack, the performance of the propeller is determined as a function of α from 2 to 12 deg. To avoid the approximation of the classical Prandtl lifting line model for the wing, the theory from Pistolesi–Weissinger[13,15] is used here. In this model, the bound vortex is placed on the wing quarter-chord line and the tangency condition to the surface is enforced at the three-quarter-chord line.

By assuming three different wing planforms, rectangular, swept-back, and elliptical as input, making the hypotheses of steady flow and negligible effects of vortex roll-up, and regarding the wake and wing to be coplanar, one obtains an integro-differential equation with the boundary condition for the wing circulation Γ = 0 at wing tips. Following Ref. 16 for the rectangular wing lifting line equation, for the swept-back wing (see Fig. 1a for the meaning of the symbols), we have

$$w(x, y, 0) = \frac{1}{4\pi}\int_{-s_0}^{0} \Gamma'(t) \times \left(\frac{1}{t-y}\left\{1 + \frac{\sqrt{[(x + t\tan\phi)^2 + (y-t)^2]}}{x + y\tan\phi}\right\} - 2\tan\phi\,\frac{\sqrt{(x^2+y^2)}}{x^2 - y^2\tan^2\phi}\right) d\eta + \frac{1}{4\pi}\int_{0}^{s_0} \frac{\Gamma'(t)}{t-y} + \left\{\frac{\sqrt{[(x - t\tan\phi)^2 + (y-t)^2]}}{x - y\tan\phi}\right\} d\eta \tag{13}$$

where $\Gamma'(t)$ represents the strength of the vortex shed from an elementary segment of the bound vortex, and $w(x, y, 0)$ is the downwash induced by the trailing vortices emanating from the starboard wing. Meanwhile, the lifting line for the elliptical wing is easily obtained from

$$c = (c_0/s_0)\sqrt{s_0^2 - y^2} \tag{14}$$

in which c and c_0 represent the wing chord related to the current coordinate y and the centerline chord, respectively. For the three cases, one may obtain the three-quarter-chord lines:

$$z_{3/4} - z_{1/4} = (c_0/2) \quad \text{(rectangular wing)} \tag{14a}$$

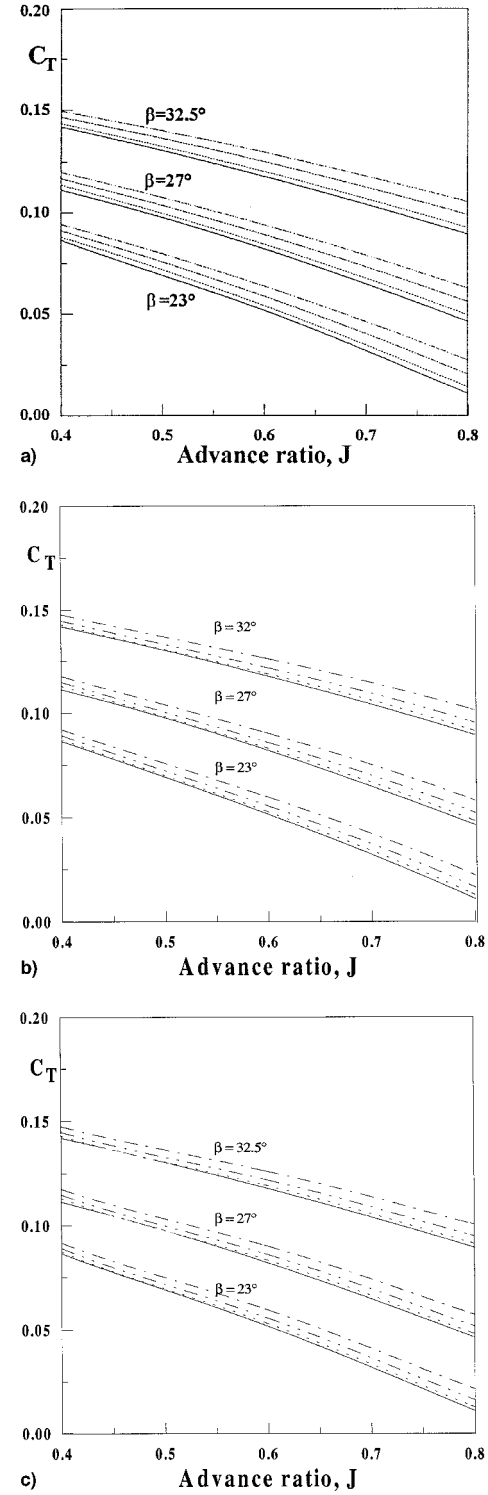

Fig. 2 a) Rectangular, b) swept-back, and c) elliptical wings. Propeller thrust coefficient: solid line, isolated; dotted line, coupled, α = 2 deg; line-2 points, α = 6 deg; and line-point, α = 12 deg.

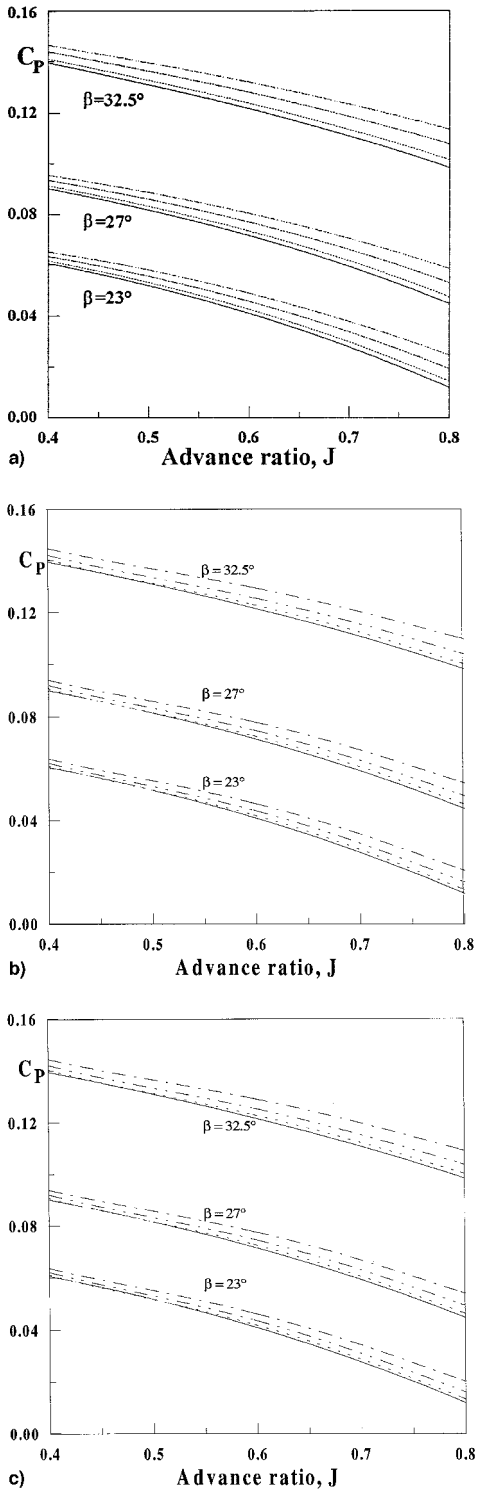

Fig. 3 a) Rectangular, b) swept-back, and c) elliptical wings. Propeller power coefficient: solid, isolated; dotted line, coupled, α = 2 deg; line-2 points, α = 6 deg; and line-point, α = 12 deg.

And for the swept-back wing, by putting into Eq. (13) the quantity

$$x = |y| \tan \phi + \tfrac{1}{2} c(y) \quad \text{(swept-back wing)} \qquad (14b)$$

where $c(y)$ is the local chord of the airfoil. When the airfoil local slope $s(\phi, t)$ is equal to w/U_∞ (with obvious meaning of symbols), Eq. (13) gives an integral relation for $\Gamma'(t)$, which in Weissinger's method is satisfied just at the three-quarter

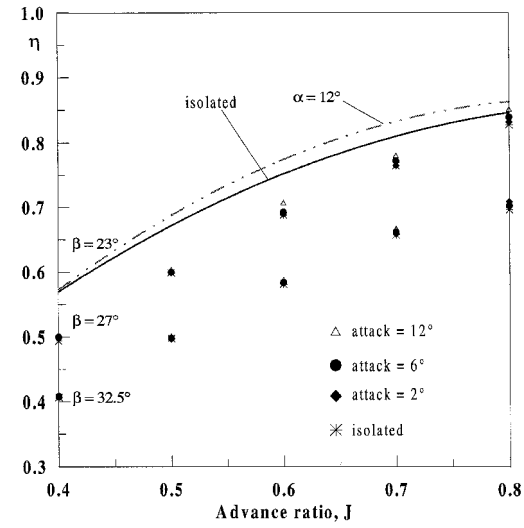

Fig. 4 Swept-back wing coupled, propeller efficiency.

chord points.[17] For the elliptical wing, remembering the previously mentioned variation law for the chord realized by a wing of elliptic planform, the equation is

$$\frac{4x^2}{c_0^2} + \frac{y^2}{s_0^2} = 1 \qquad (14c)$$

The system of wake vortices is assumed to be adequately represented by a set of vortices lying in the wing plane and parallel to the freestream and trailing from the three-quarter-chord line downstream. This set of vortices may be thought of as free when their geometry is considered as determined by using the self-induced wake velocity. For the swept case, Weissinger's method places and applies the vortex line and the boundary conditions at the same points previously mentioned for the rectangular wing and assumes the vortex line on the starboard wing has the same sweep angle. By integrating along the lifting line and by collecting the two previously mentioned contributions, one obtains the induced velocity. Once the Pistolesi–Weissinger condition between induced velocity and angle of attack has been imposed, and by normalizing the induced velocity and geometry parameters by U_∞ and the semispan x_b, respectively, the integro-differential equation is obtained:

$$2 \cdot \alpha_0(s) = \frac{1}{\pi} \cdot \int_{-1}^{1} \frac{d\Gamma w}{dt} \cdot \frac{dt}{s - t} + \frac{1}{\pi} \cdot \int_{-1}^{1} T(s, t) \cdot \Gamma w(t) \cdot dt \qquad -1 \le s \le 1 \qquad (15)$$

where α_0 is shown and $T(s, t)$ is given by

$$T(s, t) = \frac{2}{\sqrt{c^2 + 4 \cdot (s - t)^2} \left[1 + \sqrt{c^2 + 4 \cdot (s - t)^2} \right]} \qquad (16)$$

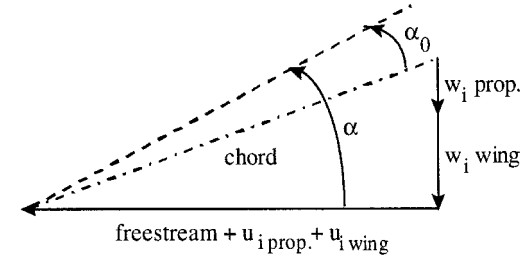

where c is the normalized wing chord, and s is the spanwise coordinate along the lifting line. The tip boundary condition

for the circulation is $\Gamma(s = -1) = \Gamma(s = 1) = 0$. On the other hand, for a swept wing, one may use (Fig. 1a for $y > 0$):

$$L(y, t) = \frac{1}{2}\frac{c}{y - t} \times \left(\frac{\sqrt{\left\{\left[\frac{1}{2}c + (y + t)\tan\phi\right]^2 + (y - t)^2\right\}}}{2y\tan\phi + \frac{1}{2}c} - 1 \right) + 2\tan\phi \frac{\sqrt{\left\{\left[\frac{1}{2}c + (y + t)\tan\phi\right]^2 + y^2\right\}}}{2y\tan\phi + \frac{1}{2}c} \quad (t < 0) \tag{17}$$

where the local lift $L(y, t)$ is related to the circulation at this point; similar expressions may be obtained for $y < 0$ and $t > 0$. For the elliptical wing, the downwash is constant and easily calculated. Suitable mathematical procedures[11,14–16] applied to both Eqs. (15) and (17) lead to a numerical solution for the circulation that can be expressed as follows:

$$\Gamma w(t) = (1 - t^2)^{1/2} \cdot \sum_{j=1}^{N} \varpi_j \cdot \frac{U_N(t)}{(t - t_j) \cdot U'_N(t_j)} \tag{18}$$

where ϖ_j are a set of unknown coefficients, and $U_N(t)$ ($N = 1, 2 \ldots$) are the Chebyshev polynomials of the second kind with t_j their zeroes.

Through the following relationships one obtains the collocation points s_k and t_j:

$$s_k = \cos\left(k \cdot \frac{\pi}{n + 1}\right), \qquad t_j = \cos\left(j \cdot \frac{\pi}{n + 1}\right) \tag{19}$$

For the rectangular planform, input wing data consist of the (constant) chord equal to 1.5 m (4.92 ft), AR = 8, wing span 12 m (39.36 ft), and the number of collocation points at which the values of circulation and the induced velocities will be calculated. For the swept and elliptical wings, the input data are the chords at the midspan l_0 and at the tips l_e, referred to the midspan coordinate y_0. We chose

$$l_0 = 0.25; \qquad l_e = 0.1 \quad \text{swept}$$

$$l_0 = 0.318; \qquad l_e = 0.0318 \quad \text{elliptical}$$

The wings have a NACA 64A408 airfoil and a negligible dihedral angle. The induced velocities calculated for the wing were input to the propeller to determine the influence of the different planform of the wings on the coefficients C_T, C_P, and η. The wing wake-induced velocities upstream of the propeller affect J, giving a chain of events starting from variations of propeller performance parameters. Assuming a fixed coordinate system (Fig. 1) X, Y, Z, and taking the X axis along the direction of the wing chord Y along the wing span, and with Z directed up, the general representation for the induced velocity field caused by the trailing vortices $d\Gamma$ leaving the finite rectangular wing span is given by[11,15]

$$\boldsymbol{q}_{\text{tot}} = \left(\frac{Z, 0, -X}{Z^2 + X^2}\right) \cdot \frac{1}{4\pi} \cdot \int_{-b}^{b} \left(\frac{Y + \mu}{\Theta} - \frac{Y - \mu}{T}\right) \cdot \frac{d\Gamma}{d\mu}\, d\mu + \frac{1}{4\pi} \cdot \int_{-b}^{b} \left[\frac{0, Z, -(Y + \mu)}{\Xi}\right] \cdot \left(1 + \frac{X}{\Theta}\right) \cdot \frac{d\Gamma}{d\mu}\, d\mu - \frac{1}{4\pi} \cdot \int_{-b}^{b} \left(\frac{0, Z, \mu - Y}{E}\right) \cdot \left(1 + \frac{X}{\Theta}\right) \cdot \frac{d\Gamma}{d\mu}\, d\mu \tag{20}$$

where

$$\Theta = \sqrt{X^2 + (Y + \mu)^2 + Z^2}$$

$$T = \sqrt{X^2 + (Y - \mu)^2 + Z^2} \tag{21}$$

$$\Xi = Z^2 + (Y + \mu)^2, \qquad E = Z^2 + (\mu - Y)^2$$

$\Gamma(\mu)$ is the wing-bound circulation, and $\mu = \cos[k\pi/(k + 1)]$ is the nondimensional coordinate along the wing span. Having reduced the integration path, integrated Eq. (20) by parts, and taken into account the boundary conditions, one obtains through suitable limit procedure an integral equation in which only the circulation and not its derivative is present:

$$\boldsymbol{q}_{\text{tot}} = \frac{\Gamma(\mu)(\mu_2 - \mu_1)}{4\pi} \cdot \int_{-b}^{b} \frac{\partial}{\partial\mu} \left(\left\{ \frac{Z, 0, -X}{Z^2 + X^2} \cdot \frac{(Y - \mu)}{T} + \left[\frac{0, Z, (Y - \mu)}{Z^2 - (Y + \mu)^2}\right] \left(1 + \frac{X}{T}\right) \right\} \right) d\mu \tag{21a}$$

Through Gaussian quadrature, the components of velocity can be finally determined where X, Y, and Z are obtained from

$$X = -\tilde{a} - l/4, \qquad Y = d + r \cdot \cos\vartheta, \qquad Z = r \cdot \sin\vartheta \tag{22}$$

where $\tilde{a}$ and $l/4$ represent, respectively, the position of the propeller disk plane and the quarter-chord with respect to the wing leading edge; d is the distance between the propeller rotational axis and $Y = 0$, r is a point on the blade radius, and θ is the instantaneous blade azimuth. For the total induced velocity caused by the swept-back wing, one may use Eq. (17). By applying Multhopp's method, the induced downwash is now a set of n simultaneous equations for the spanwise circulation functions Γ_k, in which the induced velocity is known from the boundary conditions at the wing, or in other words putting

$$\varphi = \cos^{-1} y/s_0 \tag{23}$$

$w(\varphi_k)/U_\infty$ is taken equal to the slope of the mean camber line of the wing at the three-quarter-chord point. Note that the previous fixed coordinate system X, Y, Z does not take into account the instantaneous position of the blade. Therefore, the local velocity components have been projected in a rotating coordinate system placed at a point P of the blade in such a way that q_x becomes the induced axial velocity component normal to the propeller disk plane, q_y and q_z the induced radial and tangential components, respectively. The same procedure has been made for the other two types of wing. Having found these components from the previous equations and having taken into account the radial deformation of the wake, though that is not large, one obtains the new coefficients C_T, C_P, and η. As previously described[11] for a two-bladed propeller, C_T, C_P, and η are related to J and θ, the angle of attack taken to be 2, 6, and 12 deg, and the mean blade pitch to be 23, 27, and 32.5 deg.

Results and Discussion

Figures 2a–2c, 3a–3c, and 4 show the coefficients C_T, C_P, and η both for the isolated and installed propeller. Figures 5a–5c and 6a–6c present the calculated amplitudes of the thrust and power variations, ΔC_T, ΔC_P vs θ, as a function of α and β when a basic angular frequency of 62.86 Hz is used.

From Figs. 2a–2c, 3a–3c, and 4, when $\beta = 32.5$ deg and $\alpha = 12$ deg, the thrust coefficient C_T increases by about 5% from 0.14191 to 0.14959 for the propeller installed with the wing of rectangular planform because of the interference of the wing on the propeller. Likewise, the power coefficient C_P increases by 4.9% from 0.13948 to 0.14627, and the efficiency η increases one half from 0.40753 to 0.40962 (only a picture

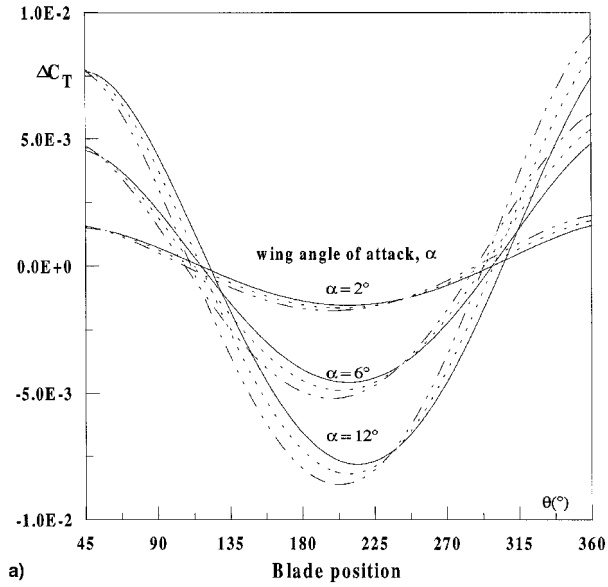

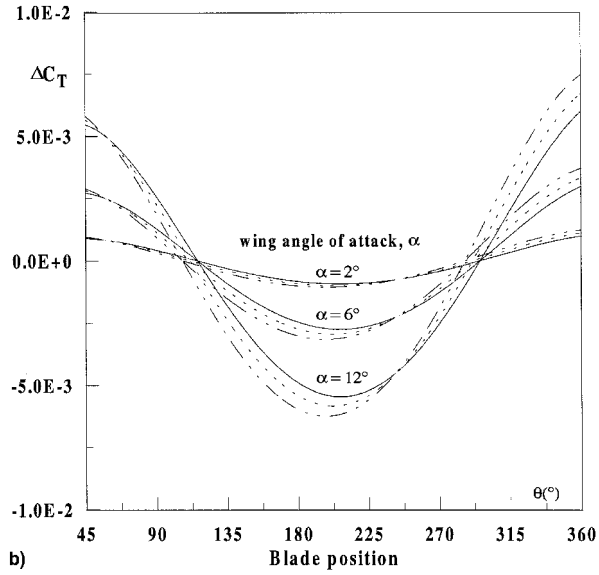

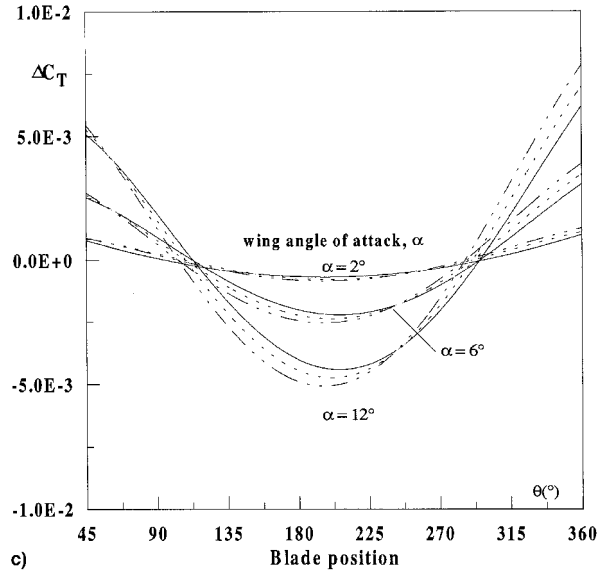

Fig. 5 a) Rectangular, b) swept-back, and c) elliptical wings. Azimuthal variation of the thrust coefficient for solid line, $\gamma = 0.4$ and $\beta = 23$ deg; dotted line, $\beta = 27$ deg; and dashed line, $\beta = 32.5$ deg.

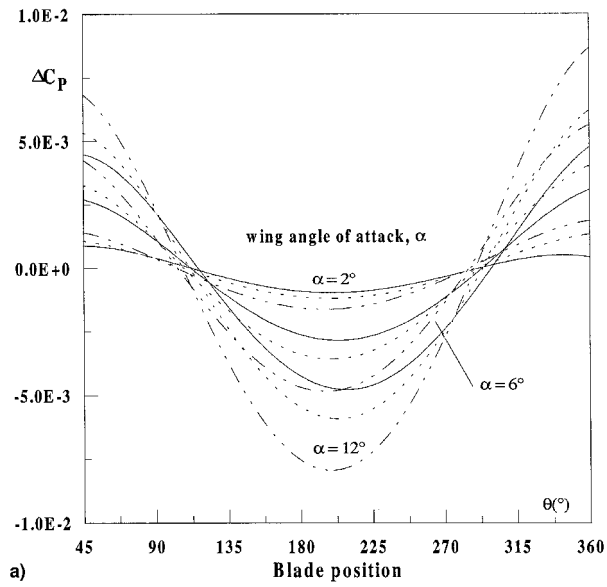

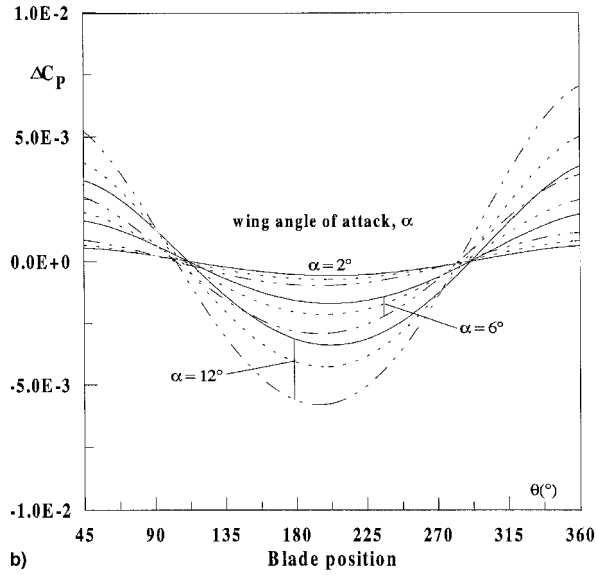

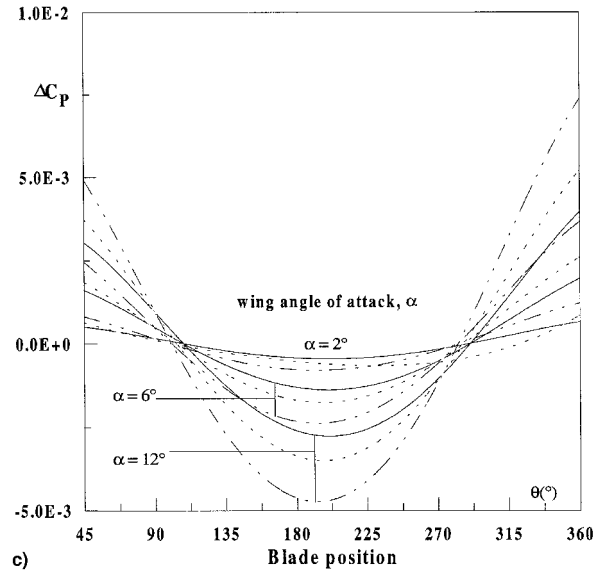

Fig. 6 a) Rectangular, b) swept-back, and c) elliptical wings. Azimuthal variation of the power coefficient for solid line, $\gamma = 0.4$ and $\gamma = 23$ deg; dotted line, $\beta = 27$ deg; and dashed line, $\beta = 32.5$ deg.

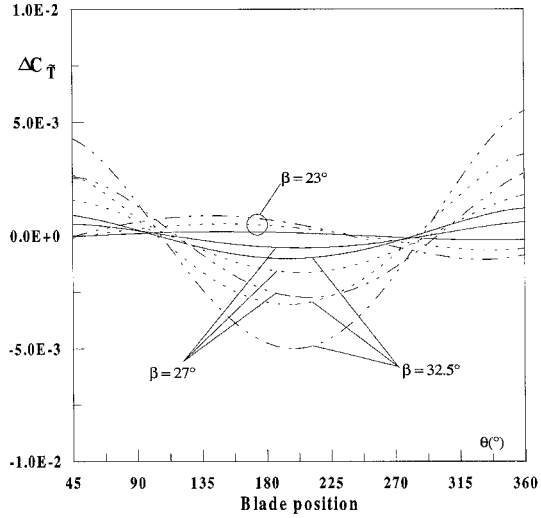

Fig. 7 Rectangular wing, vibration on the wing–propeller for dotted line, γ = 0.4 and α = 2 deg; line-2 points, α = 6 deg; and dashed line, α = 12 deg.

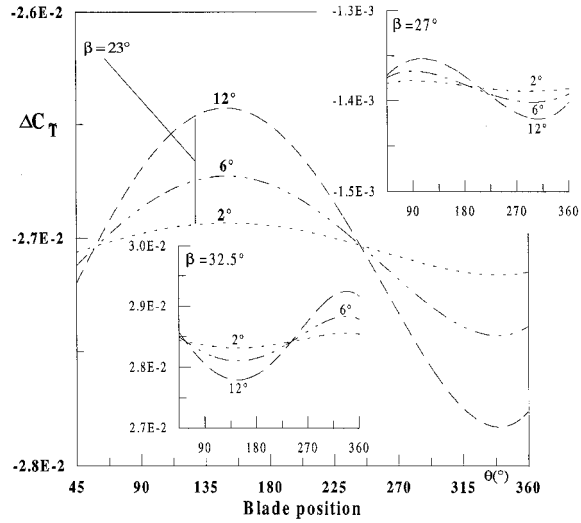

Fig. 8 Swept-back wing, vibration on the wing–propeller for dotted line, γ = 0.4 and α = 2 deg; line-2 points, α = 6 deg; and dashed line, α = 12 deg.

of η for the swept case is shown because negligible differences in efficiency are found for the different wings). The same coefficients, related to the swept-back wing, show an increase of 4.08 and 3.73% for C_T and C_P, respectively. For the elliptical wing, C_T and C_P increase 3.86 and 3.53%, respectively.

The explanation for these results is in the smaller induction that arises from the swept wing (having less area than rectangular wing) and in the constant downwash from the elliptical one. Because of the change in the velocity field, the freestream axial velocity decreases and, therefore, the advance ratio J yields an increase of the coefficients C_T, C_P, and η. Figures 2a–2c, 3a–3c, and 4 also show C_T, C_P, and η for a set of α values. Once J is fixed, the most significant variations of C_T and C_P are related to the increase in β, and these are more significant than those caused by an increase of α. Strictly speaking, the thrust is more sensitive to the change of blade pitch than angle of attack for the same flight conditions and for the same blade angular position. This is also true for the power coefficient and efficiency, although a significant variation of efficiency because of α was calculated for β = 32.5 deg. Figures 5a–5c and 6a–6c show the variations of C_T and C_P, with blade position for a given advance ratio, angle of attack, and blade pitch angle. Once β, J, and α are given, the amplitude of thrust and power are the difference, for each wing planform, between the values of C_T and C_P, with and without interference, for θ. Additional observations for each case are in the following text.

Rectangular Wing

The amplitude of C_T decreases between θ = 45 and 225 deg and increases between θ = 225 and 0 deg. The same conclusions may be deduced from the point of view of power; the efficiency curves are omitted because their difference in values is negligible. The values of C_T are not perfectly periodic with θ because the wing wake is not symmetrical behind the propeller. From Figs. 5a–5c and 6a–6c it may be seen that the largest values of ΔC_T and ΔC_P are associated with increasing α and β. It is worth noting that, even though the largest variations of thrust and power are associated with the largest α and β, these occur within a relatively small range of θ (120–240 deg); however, at lower values of α and β these persist for a longer period θ (60–360 deg). To explain this oscillation in thrust, one has to look at the effect of the position of the blade. For a given α and β, when the two blades are in vertical position (90 ± 15 deg), in contrast to the horizontal position, the wing-induced velocities, which are changing not only

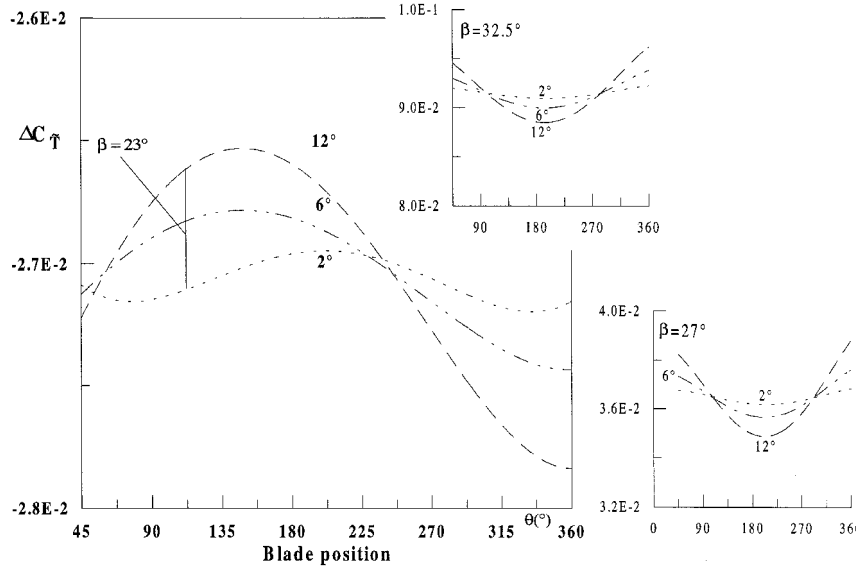

Fig. 9 Elliptical wing, vibration on the wing-propeller for dotted line, γ = 0.4 and α = 2 deg; line-2 points, α = 6 deg; and dashed line, α = 12 deg.

along the wing span but also orthogonal to the wing leading edge, will influence the asymptotic condition of flow even more. It should also be noted that for two values of θ, 112 and 112 deg + π, the variation in C_T and C_P vanishes (the set of curves merge).

Swept-Back Wing

The amplitude of C_T decreases between θ = 45 and 200 deg and increases between θ = 200 to 360 deg, showing a phase difference: −25 deg in decreasing and +25 deg in increasing. The same conclusions may be deduced from the point of view of power; but here a phase coincidence may be seen between the two cases. For the same reason of the rectangular case, the efficiency curves are omitted. From Figs. 5b and 6b it may be seen that the smaller induction has as effect lower amplitudes of ΔC_T and ΔC_P for the same range of angular position. The variations of thrust and power are gradually reducing, and at lower values of α and β these persist for a larger range of θ than the rectangular case.

Elliptical Wing

Because of the constant downwash velocity component, as displayed in Figs. 5c and 6c, we found the amplitudes of ΔC_T and ΔC_P, for the same range of angular position. ΔC_T and ΔC_P show a gradual reduction in amplitude, while they persist for a wider range of blade azimuthal positions than those previously described. Finally, to display the thrust oscillations as sources of vibration on the aircraft, Figs. 7–9 show the variation of $\Delta C_{\bar{T}}$ against θ, where $\Delta C_{\bar{T}} = C_T(\theta)_{\text{with interference}} - C_T(\theta)_{\text{average with interference}}$ for the different types of wing considered.

Conclusions

A numerical methodology has been presented for solving the aerodynamic problem of the characteristics of a propeller mounted in front of a wing having different planforms. The approach that is presented shows a numerical evaluation of the interference of the different induced velocity fields caused by the presence of three different types of wings and its effect on a tractor propeller and its performance. Some improvements of the method may be obtained by checking the effects of the interference of the variations of C_T and C_P on the dynamics of the complete aircraft, e.g., the interaction of ΔC_T on the pitching frequency and the effects of changes in the wing aerodynamic center. From the numerical point of view, more effectiveness may be reached when the new wing loads distribution along the wing span are evaluated and put in relation to the altered upstream conditions. For this, a more convenient lifting surface panelization for the wing should be adopted.

Acknowledgments

The author is indebted and grateful to Gianfranco Chiocchia of the Aerospace Department of Politecnico of Torino, who highlighted the significance of the wing–propeller interaction, and to Michael A. McVeigh of the Boeing Helicopters Division of Philadelphia. His previous help was invaluable to the writer. Special thanks to Giovanni Lombardi and Guido Buresti of the Aerospace Engineering Department of Pisa, and Daniel Favier and Christian Maresca of Institute de Recherche sur les Phenomenes Hors Equilibre (I.R.P.H.E.) of Marseille, France for their useful comments and exchange of ideas, and to Giuseppe Davì of the author's former Department for his encouragement.

References

[1]Witkowski, D., Lee, A., and Sullivan, J., "Aerodynamic Interactions Between Propellers and Wings," *Journal of Aircraft*, Vol. 26, No. 9, 1989, pp. 829–836.

[2]Cho, J., and Williams, M. H., "Propeller-Wing Interaction Using a Frequency Domain Panel Method," *Journal of Aircraft*, Vol. 27, No. 3, 1990, pp. 196–203.

[3]Rottgermann, A., and Wagner, S., "Compressible Potential Flow Around a Helicopter Rotor," *Computational Mechanics*, Vol. 2, Springer–Verlag, New York, pp. 2915–2920.

[4]Catalano Martini, F., "The Aerodynamic Characteristics of a Smooth Wing at Low Reynolds Number Under Effect of a Pusher Propeller," *Proceedings of the Symposium COBEM-CIDIM'95* (Belo Horizonte, Brazil), Microservice, Sao Paulo, Brazil, 1995.

[5]Kinnas, A. S., and Hsin, C. Y., "Boundary Element Method for the Analysis of the Unsteady Flow Around Extreme Propeller Geometries," *AIAA Journal*, Vol. 30, No. 3, 1992, pp. 688–696.

[6]Yamaguchi, H., and Bose, N., "Oscillating Foils for Marine Propulsion," *Proceedings of the 4th International Offshore and Polar Engineering Conference*, Vol. 3, International Society of Offshore and Polar Engineers, Osaka, Japan, pp. 539–544.

[7]Bose, N., "Performance of Chordwise Flexible Oscillating Propulsors Using a Time-Domain Panel Method," *International Shipbuilding Progress*, Vol. 432, No. 42, 1995, pp. 281–294.

[8]Favier, D., Ettaouil, A., and Maresca, C., "Numerical and Experimental Investigation of Isolated Propeller Wakes in Axial Flight," *Journal of Aircraft*, Vol. 26, No. 9, 1989, pp. 837–846.

[9]Favier, D., and Maresca, C., "Etude du Sillage 3D d'une Hélice Aérienne Quadripale," *AGARD FDP on Aerodynamics and Acoustics of Propellers*, CP-366, Oct. 1984 (Paper 15).

[10]Favier, D., Nsi Mba, M., Barbi C., and Maresca, C., "A Free-Wake Analysis for Hovering Rotors and Advancing Propellers," *Proceedings of the 11th European Rotorcraft Forum* (London), 1985, pp. 493–511.

[11]Ardito Marretta, R. M., and Lombardo, G., "Coefficienti di Trazione, di Coppia e Rendimento dell'Elica in Presenza del Campo Aerodinamico di un'Ala Finita," *Aerotecnica–Missili e Spazio*, Vol. 73, Nos. 1, 2, 1994, pp. 31–41.

[12]Chiaramonte, J. Y., Favier, D., Maresca, C., and Benneceur, S., "Aerodynamic Interaction Study of the Propeller/Wing Different Configurations," *Journal of Aircraft*, Vol. 33, No. 1, 1996, pp. 46–53.

[13]Weissinger, J., "Uber die Auftriebverteilung von Pfeilflugen," Zentrale fur wissenschaftliches Berichtswesen der Luftfahrtforschung des Generalluftzeug-meisters No. 1553, Berlin-Adlershof, 1942.

[14]Prossdorf, S., and Tordella, D., "On an Extension of Prandtl's Lifting Line Theory to Curved Wings," *Impact of Computing in Science and Engineering*, Vol. 3, Jan. 1991, pp. 192–212.

[15]Chiocchia, G., and Pignataro, S., "On the Induced Drag Reduction Due to the Propeller-Wing Interaction," *Aeronautical Journal of the Royal Aeronautical Society*, Vol. 99, No. 988, 1995, pp. 328–336.

[16]Ardito Marretta, R. M., "Performance of a Propeller Embedded in the Flowfield of a Wing," *Journal of Aircraft*, Vol. 33, No. 5, 1996, pp. 919–923.

[17]Robinson, A., and Laurmann, J. A., "Wing Theory," *Cambridge Aeronautical Series*, 1st ed., Vol. 2, Cambridge Univ. Press, Cambridge, England, UK, 1956, pp. 28–36.